



Wind-wave transformations in an elongated bay

Hande Caliskan, Arnaldo Valle-Levinson*

Civil and Coastal Engineering Department, University of Florida, 365 Weil Hall, Gainesville, FL 32611-6580, USA

ARTICLE INFO

Article history:

Received 10 July 2007

Received in revised form

10 March 2008

Accepted 14 March 2008

Available online 19 March 2008

Keywords:

Wave transformations

Concepcion Bay

Gulf of California

ABSTRACT

In order to determine wave transformations in an elongated bay, a numerical solution was used to interpret yearlong records of bottom pressure and wind velocity obtained at the mouth and head of Concepción Bay, on the Gulf of California side of the Baja California peninsula. Observed wind waves were predominantly produced by southeastward winds in the winter and north–northwestward winds in the summer. Typical mean wave periods at the bay entrance were between 3 and 5 s. In contrast, the waves at the head of the bay had predominant periods <3 s. The energetic long-period swell waves were dissipated somewhere in the bay as they were not observed at the head of the bay. This study centered in identifying the effects that caused swell waves to attenuate in the bay. The ‘Simulating WAVes Nearshore (SWAN)’ model was used to determine the cause for such wave attenuation. Model results showed that swell waves were attenuated because of the combined effects of bottom friction, wave breaking, whitecapping, refraction and wave blocking by the coastline. Most of the attenuation (close to 90%), however, was caused by wave blocking owing to the change of coastline orientation of the bay. This wave blocking mechanism should therefore be explored further in embayments of complex coastline morphology.

© 2008 Published by Elsevier Ltd.

1. Introduction

The study of wave transformations in semienclosed basins has been addressed at different sites around the world (e.g. Boon et al., 1996; Wu and Thornton, 1989; Soomere, 2005). One of the common findings in these studies has been the observation that ocean swell vanishes at some distance into a bay. Boon et al. (1996) observed that in Chesapeake Bay, ocean swell waves were attenuated before they reached the middle of the bay. Soomere (2005) noted a similar situation in Tallinn Bay, Estonia, and attributed it to refraction and wave breaking over shallow banks. Ts'o and Barsky (1987) argued that wave heights in bays become small because of refraction, but Smith et al. (2001) ascribed wave height attenuation in the shallow Manukau Harbor, New Zealand, to bottom friction.

The attenuation of swell waves has also been widely documented in open coasts (e.g. Long, 1973; Abreu et al., 1992; Thornton and Guza, 1983). Furthermore, Ardhuin et al. (2003a) and Long and Oltman-Shay (1991) observed that ocean swell waves attenuated at the open coast of Virginia and North Carolina, USA. Wave frequency was higher and direction was nearly perpendicular to the bottom contours as waves approached the coast. Long and Oltman-Shay (1991) hypothesized that the cause of the attenuation of ocean swell waves at open coasts was refraction,

while Ardhuin et al. (2003a) attributed such attenuation primarily to bottom friction and occasionally to refraction. Additionally, wave attenuation can be caused by blocking from opposing currents in the vicinity of tidal inlets (e.g. Shyu and Phillips, 1990; Chawla and Kirby, 2002) and by island blocking (e.g. Pawka et al., 1984). To our knowledge, refraction has been the main mechanism proposed to explain the reason for swell attenuation in embayments (e.g. Soomere, 2005; Ts'o and Barsky, 1987).

This study is motivated by the observation that low-frequency waves (periods >5 s) were dissipated inside Bahía Concepción, an embayment on the Gulf of California side of the Baja California peninsula in México (Fig. 1). *In-situ* data recorded at the bay entrance and at the head of the bay suggested the influence of waves with periods of 4–5 s at the entrance but waves with periods <3 s at the head (Fig. 2). The main purpose of that data collection was to determine along-bay pressure gradients and not wave transformations in the bay. Data were recorded according to the requirements of such main purpose and did not have appropriate temporal coverage to yield a fully reliable set to determine wave climatology or to determine wave transformations. Nonetheless, the data suggested the process of wave attenuation in the bay. In order to test the concept of wave attenuation in Bahía Concepción, a numerical wave model was used to (a) validate the reliability of the waves data, (b) find the possible reasons behind the attenuation, and (c) assess the contribution of various dissipating effects on attenuation.

The study area is located in the Gulf of California side of the Baja California peninsula between the longitudes of $-111^{\circ}58'8''$

* Corresponding author. Tel.: +1 352 392 9537.

E-mail address: arnaldo@ccpo.odu.edu (A. Valle-Levinson).

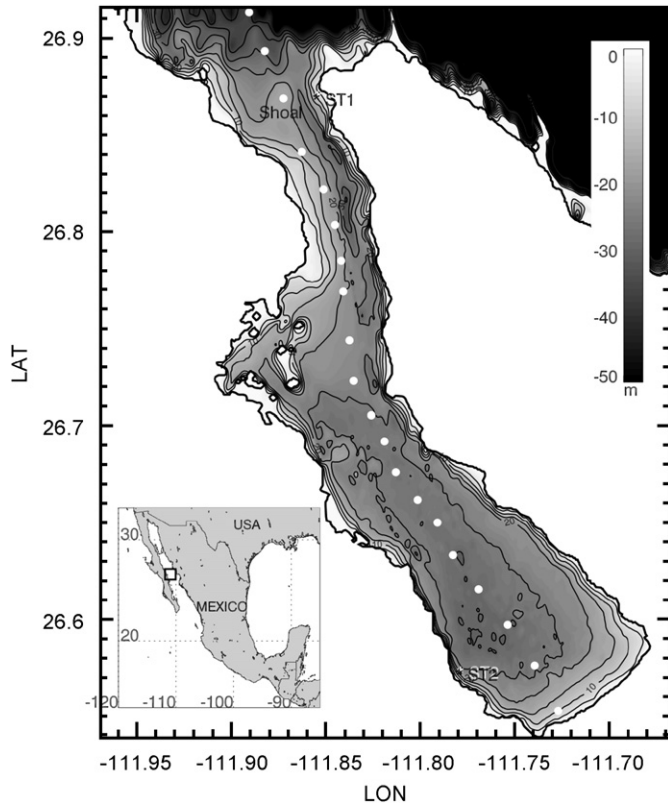


Fig. 1. Bahía Concepción in the context of the Gulf of California and measurement stations ST1 and ST2. The bathymetric distribution of the bay is contoured at 5 m intervals. The white, filled circles indicate the position for which wave energy density is calculated.

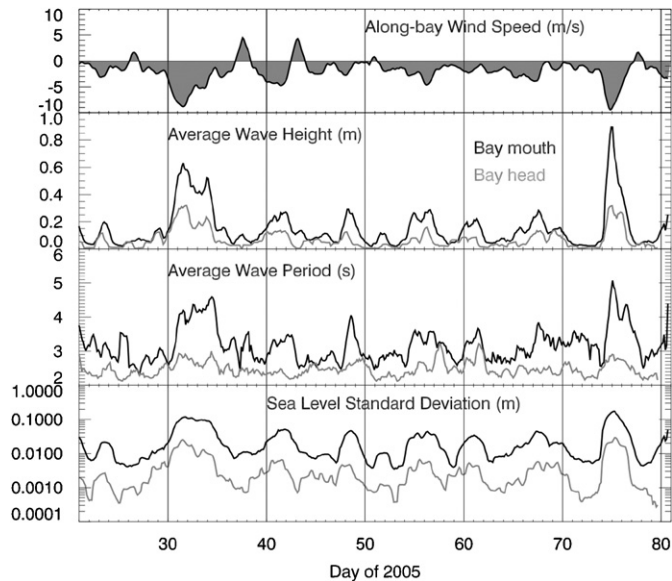


Fig. 2. Along-bay wind speed (negative is toward the head), average wave height, average wave period and sea level standard deviation at the mouth and head of Concepción Bay during a selected period between January and March 2005. In the 3 lowermost panels, the darkest line represents the record at the bay mouth (ST1). The highest and longest waves developed during the strongest winds toward the bay head.

and $-111^{\circ}40'6''$ and the latitudes of $26^{\circ}32'21''$ and $26^{\circ}54'57''$ (Fig. 1). Bahía Concepción is exposed to northwesterly winds, blowing along its axis, with speeds > 10 m/s for extended periods

during winter and spring (Badan-Dangon et al., 1991). In the summer, winds are predominantly from the south and tend to be weaker than autumn and winter winds. There is no published information on the wave climatology in the Gulf of California in the region off the mouth of Concepción Bay. However, the steady direction of the winter winds in the Gulf of California produces waves with restricted directional spread, typical heights of 1–2 m and periods of 10 s just outside the bay (Gutiérrez de Velasco, personal communication).

The bay's bathymetry is relatively simple. Immediately after the bay entrance, there is a deep and narrow channel with an average depth of 30 m on the east side of the bay mouth. The deepest point of the bay is located in this channel and the depth there approaches 35 m. The bay entrance, with a width of 6 km, is located 40 km away from its south end point. The bay width varies between 3.4 and 10.4 km. The west side of the bay, close to the entrance, has the mildest bed slope causing an extended shallow zone from the coast. In the shallow zone of the middle of the bay, between the latitudes of $26^{\circ}42'31''$ and $26^{\circ}45'13''$ there are several islands: Isla San Ramon, Isla Pitahaya, Isla Blanca, Isla Bargo, Isla Guapa and Isla Tecomate. The islands keep the west and middle side of the bay relatively sheltered from winter winds.

2. Approach

Bottom pressure values were recorded every 15 min at the mouth and head of the bay (Fig. 1) with the original purpose of determining along-bay pressure gradients (not reported here). These measurements were obtained between November 2004 and October 2005. Data were recorded with SeaBird SBE26 wave and tide recorders equipped with 45 psi Paroscientific pressure sensors. Instruments were deployed at a depth of 5.10 m at the entrance (ST1) and of 5.70 m at the head (ST2) of the bay (Fig. 1). At the same time, wave data were recorded with a frequency of 4 Hz at 30 s bursts every 3 h (instrument's default). Wind velocities were recorded using Aanderaa anemometers at a frequency of 1 Hz. The anemometers were deployed at a height of 10 m above mean sea level at the entrance and the head of the bay, at distances of < 1 km from the bottom pressure recording stations ST1 and ST2.

In order to assess whether the wind wave patterns suggested by observations were reliable, the Simulating WAVes Nearshore Model (SWAN Model) was applied to the bathymetry of Concepción Bay. The SWAN Cycle III version 40.41 was used for this study (Booij et al., 1999; Ris et al., 1999). Model inputs were bathymetry, wind velocity and wave forcing. A southeastward wind of 10 m/s was used as the base case (BC1), typical of winter conditions. In addition, waves were prescribed at the northern boundary of the domain with an approach angle consistent with the wind prescribed, a directional spreading standard deviation of 5° , a wave height of 1.5 m and a wave period of 10 s. The reason for prescribing waves with these parameters was to represent ocean swell (remote waves) at the bay mouth. This enabled observation of the changes occurring to the waves from the mouth to the head of the bay. Prescribed waves with higher directional spreading (standard deviation of 25° and 50°) caused insignificant modifications to the wave height and direction inside the bay (Fig. 3). Directional spreading caused changes to the wave height, but not to the direction, appreciable only outside the bay in regions beyond the scope of this study. The wave directional resolution for the model output was 5° and the wave frequency resolution was logarithmically distributed in 40 values that extended from 0.05 to 0.5 Hz.

For all cases (unless otherwise noted), nonlinear quadruplet wave interactions, depth-induced wave breaking, whitecapping,

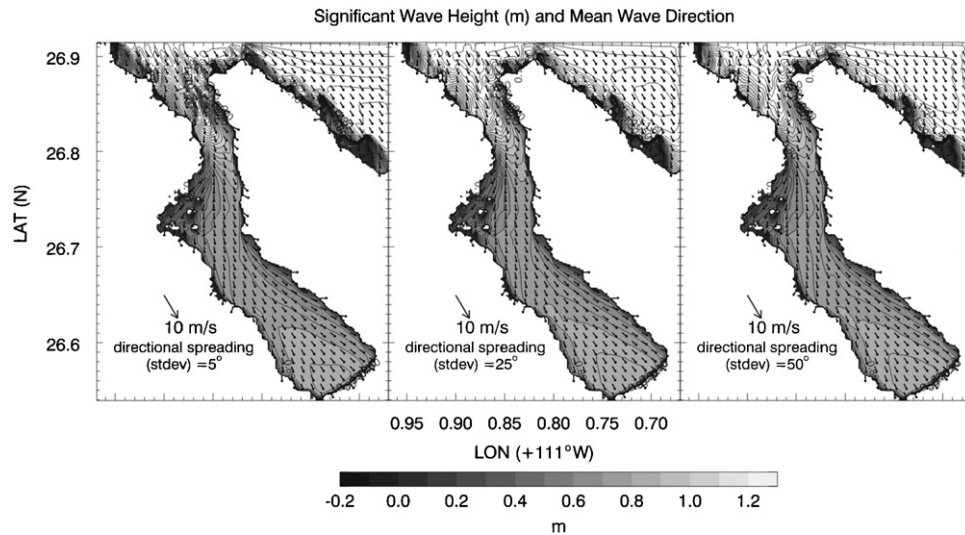


Fig. 3. Significant wave height (contours at intervals of 0.05 m) and mean wave direction (vectors in °T) for the base case (BC1) with different degrees of wave spreading. Inside the bay, the variables are essentially independent of prescribed wave directional spreading. The vectors only show direction (not scaled to their magnitude).

bottom friction and wind generation were active to try to emulate realistic conditions. Bottom friction was parameterized with the empirical JONSWAP model (Hasselmann et al., 1973), which is default. This formulation produced essentially the same results (significant wave height and energy dissipation) as the eddy viscosity approach of Madsen et al. (1988) and the drag law model of Collins (1972). Besides, the JONSWAP bottom friction parameterization is easy to use in practice because it requires no prior knowledge about bottom sediments (Ardhuin et al., 2003b).

A sensitivity test to determine the adequate spatial resolution for the model was conducted with three different grid sizes selected for the same wind speed and direction. The model was run with grid sizes of 100, 200 and 400 m both in the x and y directions. The original bathymetric data had a resolution of 35 m in x and 70 m in y . When compared to the finest grid (100 m), the 400 m grid size was unable to resolve details properly, especially along the shore (not shown). On the other hand, the grid size of 200 m caused better resolved results than the 400 m grid, showing enough details for the purpose of this study. As the grid size increased, the significant wave height also increased slightly. The difference of significant wave heights between the grid sizes of 100 and 200 m was less than 1%, whereas between 100 and 400 m the difference increased to 4% along the mid-axis of the bay. Moreover, using a grid size of 400 m caused the islands between the longitudes of $-111^{\circ}54'8''$ and $-111^{\circ}51'43''$ and the latitudes of $26^{\circ}42'31''$ and $26^{\circ}45'13''$, to disappear. A grid size of 200 m was not only able to show enough details for the purpose of this study, but it also ran in 4% of the time relative to the 100 m grid size for each simulation. The grid size of 200 m resulted in a domain of 150 grid points in x and 210 points in y . This grid was chosen for the rest of the experiments because it met the requirements for both time efficiency and wave propagation accuracy.

After determining the grid size, different cases for different wind speeds and directions were run. The main purpose of these tests was (a) to compare the behavior of waves at ST1 and ST2, where observations were available; (b) to compare different model results with the available observational data; and (c) to describe the behavior of waves under different wind velocities. First of all, the sensitivity of wave parameters, such as significant wave height, mean wave period and mean wave direction, to wind speed was tested with a fixed wind direction toward 150°T (i.e., from 330°T) and wind speeds of 5, 10 and 15 m/s. Second, the sensitivity to wind direction was tested with a wind speed of

Table 1
Model simulation cases

Name of the case	Wind speed (m/s)	Wind direction (°T)
BC1	10	150
BC2	5	150
BC3	15	150
BC4	10	180
BC5	10	120
BC6	10	50
BC7	10	20
BC8	10	90
BC9	10	0

The direction of the wind indicates its destination, i.e., a 150°T wind is a southeastward wind.

10 m/s and various directions. All cases simulated are summarized in Table 1 and the model results are compared to the base case BC1.

3. Results and discussion

This section contains two parts. In the first part, the results derived from data collected by the bottom-mounted instruments are presented briefly. The observations suggest that swell waves, with periods >7 s, are filtered out in the bay. The second part, which is the main part, includes detailed model results and a comparison of them with the observational results. Model results confirm the swell dissipation suggested by the observations and identify the process of blocking by the coastline as the main reason for such dissipation.

3.1. Observations

Wind velocities were low-pass filtered with a Lanczos filter with a half-power of 34 h, while average wave heights (m), wave periods (s), and sea level standard deviations (m) were obtained for each 3-h burst (Fig. 2). As the data suggest, wave action increased with along-bay wind speed toward the head of the bay (negative wind speed values in Fig. 2). The figure clearly shows that average wave periods were between 3 and 5 s at the bay mouth and <3 s at the bay head. Wave heights and sea level

standard deviations were also markedly greater at the mouth than at the head (Fig. 2). These data showed that wave energy decreased into the bay, relative to its mouth, and concentrated mostly in short period (<3 s) waves. The predominance of longer waves at the mouth than at the head of the bay is illustrated in Fig. 2 only for the period January 21, 2005–March 22, 2005. This predominance, however, was observed throughout the year, independently of the wind direction.

The reduced wave activity at the head of the bay is either caused by transfer or by loss of wave energy. The reasons for that loss or transfer may be attributed to refraction, shoaling, bottom friction, whitecapping or any combination thereof (e.g. Soomere, 2005; Smith et al., 2001). In order to verify whether low-frequency waves are dissipated at the bay and to determine the mechanism(s) responsible for that wave transformation, the SWAN wave model was applied. The results obtained from the model experiments suggested another mechanism for wave attenuation in a bay, namely wave blocking. Such results are presented next.

3.2. SWAN wave model results

Wave transformations throughout the axis of the bay were determined with one-dimensional spectral energy density ($\text{J}/\text{m}^2/\text{Hz}$) distributions at the 20 points shown in Fig. 1. These distributions were plotted as a function of frequency, in the range 0.05–0.5 Hz, and distance from the bay head. All distributions, regardless of wind speed and direction, show that the highly energetic long waves attenuate as they propagate toward the head (Fig. 4). At a distance of ~ 15 km from the mouth (or 28 km from the head), most of the low-frequency waves (<0.15 Hz) dissipate in all cases. On the other hand, higher frequency waves (>0.3 Hz) exist everywhere along the bay. This wave behavior was consistent with the observations.

As mentioned in the *Approach* section, cases BC1–BC3 were run to assess the response of the bay to wind speed change under the same wind direction and remote wave forcing conditions. The distributions of spectral energy density for these cases are shown in Fig. 4. One of the major differences for these three cases is the frequency range of energetic waves at the head of the bay. The frequency range at the head of the bay increased as the wind speed increased. For BC1, where the wind speed was 10 m/s, the waves with energies $>10^2 \text{ J}/\text{m}^2$ that reached the bay head were in the range between 0.18 and 0.50 Hz, i.e., an interval of 0.32 Hz. For BC2, the wind speed was 5 m/s and the frequency of waves with energies $>10^2 \text{ J}/\text{m}^2$ that reached the head ranged between 0.28 and 0.50 Hz, i.e., a range of 0.22 Hz. The frequency range for BC3 (wind speed of 15 m/s) was between 0.14 and 0.50 Hz, or an interval of 0.36 Hz. This indicated that stronger winds can generate waves with a wider range of frequencies reaching the bay's head, as compared to weaker winds.

The response of the bay to wind direction changes is also illustrated in Fig. 4. When the bay was under the effect of southward–southeastward winds (BC1, BC4 and BC5), the spectral energy densities along the bay were very similar to each other. The only difference was in the details of the locally generated short wind waves (frequency >0.2 Hz). When the wind blew between northward and eastward (BC6–BC9), the remote waves were forced in the same direction. That is why no low-frequency waves entered the bay at all. However, in cases of prescribing southward waves at the bay mouth combined with northward or eastward winds inside the bay, the low-frequency waves were also dissipated within the first 10 km of the bay. These situations (not shown) have low probability of occurrence in Concepción Bay but may develop during passage of cyclones. The rapid dissipation of low-frequency waves in these situations must be caused by the

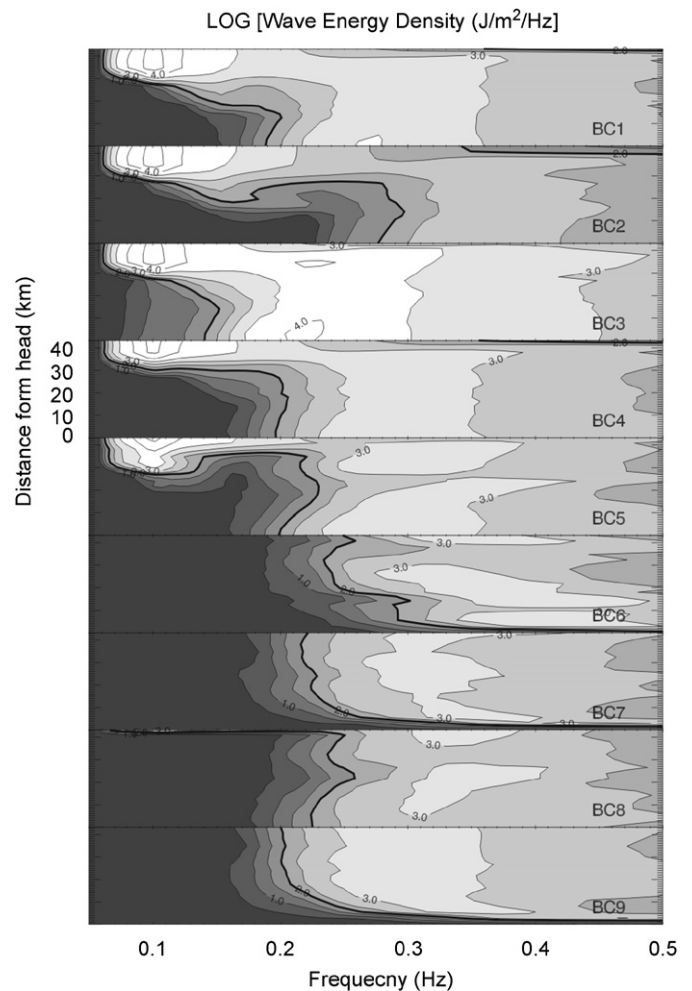


Fig. 4. Wave energy density contours (in J/m^2) as a function of their frequency distribution (x -axis) and distance throughout the bay at the locations shown in Fig. 1 (y -axis) for simulations BC1 through BC9. The logarithm of the values is contoured at intervals of 0.5 ($10^{0.5} \text{ J}/\text{m}^2$). The thickest contour represents the value of 2 ($100 \text{ J}/\text{m}^2$) to track the limit of energetic waves. The most energetic waves ($10^4 \text{ J}/\text{m}^2$) at 0.1 Hz are filtered out from reaching the head of the bay (0 km in the y -axis).

effect of the wind opposing the direction of prescribed waves at the bay mouth (Mitsuyasu, 1997).

Because the model results brought some reliability to the observational results, the SWAN model results were also used to determine the reasons for attenuation of the low-frequency waves as they propagated toward the head. The significant wave height, the mean wave direction, the average wave period and the energy dissipation outputs were used both for reinforcing the observational results and helping to find an explanation for what has been observed.

Significant wave height (H_s) distributions show that, for all cases of southward wind prescription, H_s decreased from the mouth to a distance of 6 km into the bay (Fig. 5). This attenuation mainly occurred on the western side of the bay entrance. The 30 m deep channel on the east side of the entrance did not have a significant effect on H_s attenuation. Further into the bay, H_s increased slightly for southward and southeastward winds (cases BC1, BC3 and BC5) because the wind caused waves to grow along the longest fetch in the bay. Although the wind direction for BC2 (wind speed = 5 m/s) was the same as BC1, BC3 and BC5, there was a decrease in H_s . This indicates that the wind needs to be above a certain threshold for its growing effects not to be

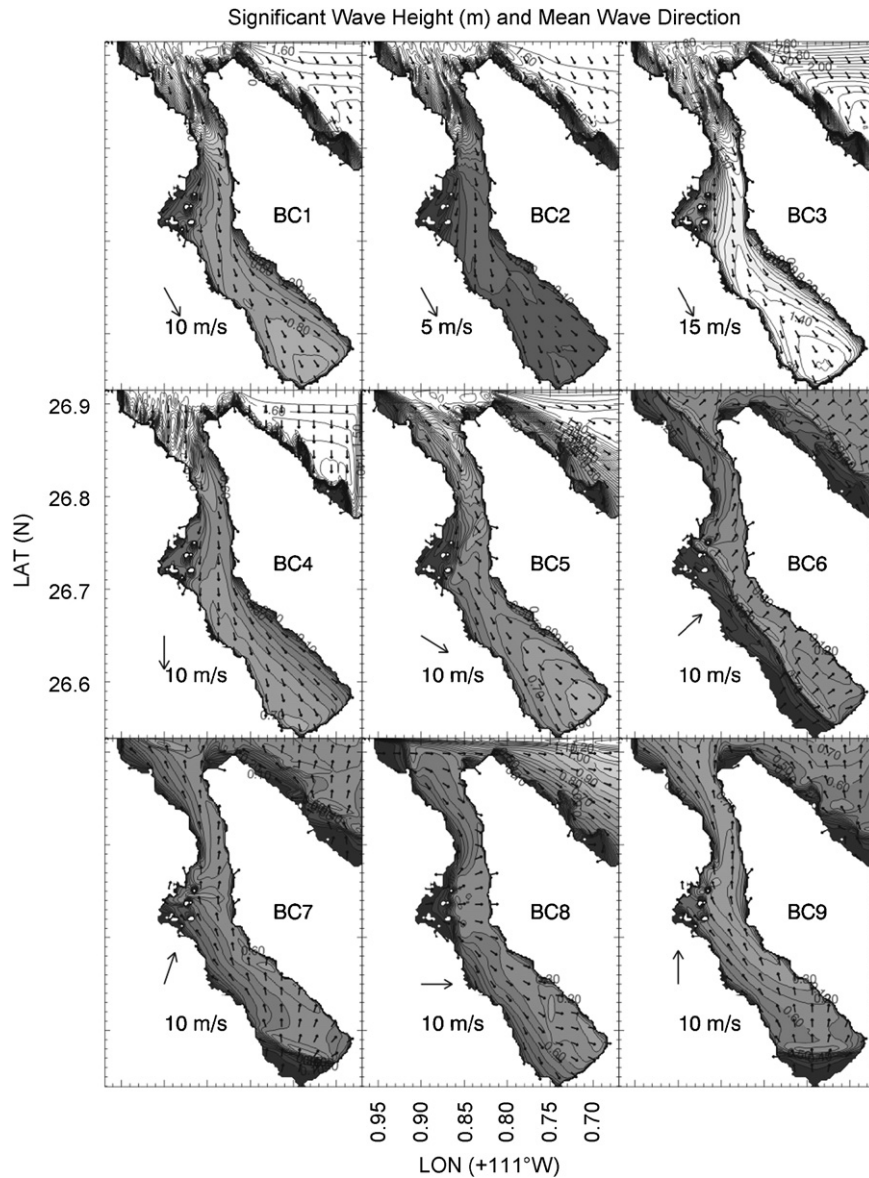


Fig. 5. Significant wave height (contours at intervals of 0.05 m) and mean wave direction (unscaled vectors in °) for cases BC1 to BC9. Wind velocities corresponding to each case are shown. Wave heights attenuate rapidly after they enter the bay in BC1 to BC5.

neutralized by attenuating effects such as refraction, diffraction and bottom friction. This threshold was identified between 5 and 10 m/s for a southward wind. When the wind blew from other directions, H_s decreased toward the head. For cases BC6 to BC9, the highest H_s was observed in the middle of the bay. In general, H_s became larger throughout the bay as wind speed increased (Fig. 5) because of the effect of wind speed on wave generation and growth (Jeffreys, 1924). Also in general, there are regions in the bay where H_s is < 0.2 m when the wind direction is not aligned with the swell propagation direction. The areas of relatively small waves (darkest areas in Fig. 5) depend mainly on the magnitude of the northward component of the wind. If the northward component dominates, as in cases BC7 and BC9, a low wave energy area is located to the SW of the bay. If the eastward component starts to dominate, as in BC6 and BC8, this area of low wave energy elongates toward the NW into the islands.

The mean wave direction distributions suggest patterns of refraction and diffraction (Fig. 5) as the wave direction conforms to the bathymetry and morphology of the bay. It appears that

SWAN can replicate refraction and diffraction patterns, even around the islands. The contribution of refraction to the low-frequency wave attenuation will be presented later on in this section. Such wave attenuation is seen clearly not only in the spectral energy density distributions (Fig. 4) but also in the patterns of wave period (Fig. 6). In the deep channel on the east side of the bay mouth, the wave period change is not as large as it is on the west side. The long periods that appear at the bay mouth disappear a few kilometers into the bay. The pattern of wave periods at the bay mouth may suggest that swell attenuation is related to bathymetry, as will also be investigated later on in this section. The wave periods in the southern part of the bay, south of the islands, change insignificantly relative to the changes in the northern third of the bay. In general, the values of the mean wave periods are consistent between simulations and observations.

Energy dissipation (W/m^2) distributions throughout the bay (Fig. 7) result from the superposition of various processes: depth-induced wave breaking, bottom friction and whitecapping. The distributions illustrate similarities between energy dissipation

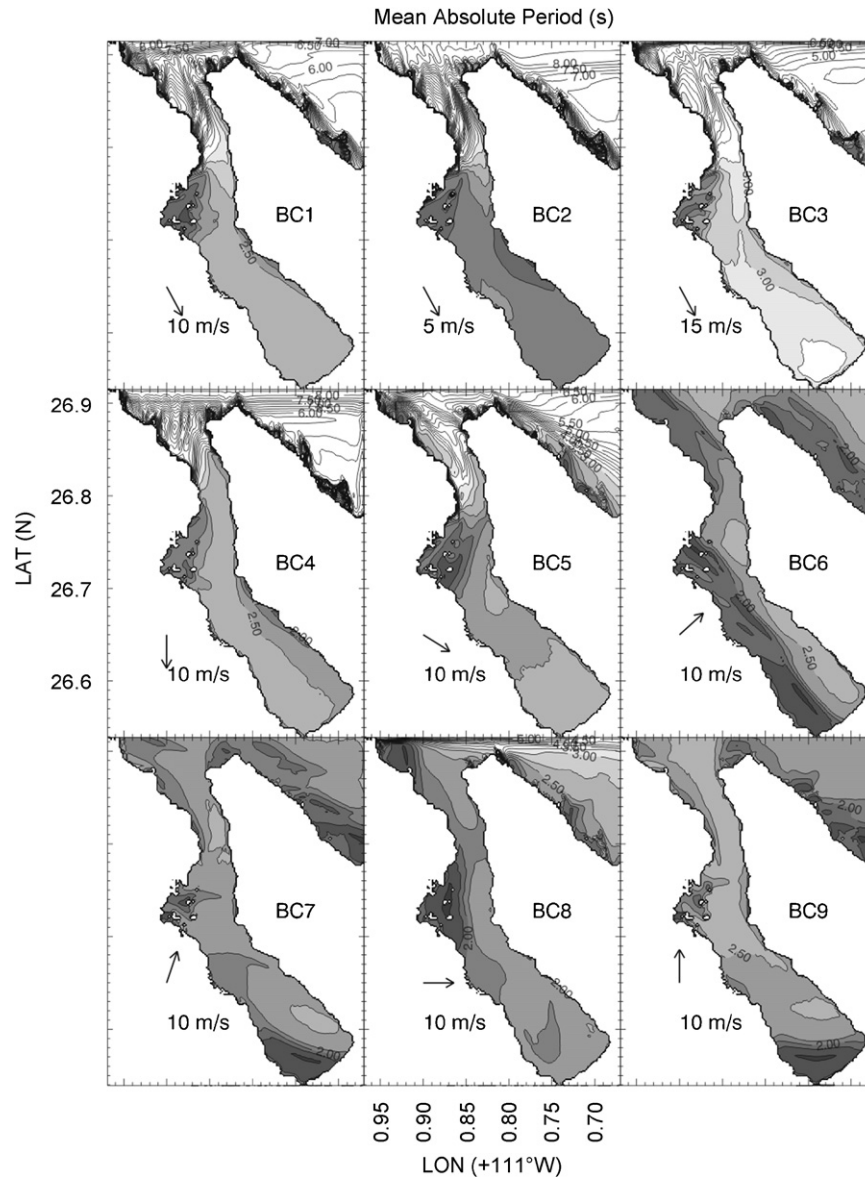


Fig. 6. Mean absolute period (contours at intervals of 0.5 s) for BC1–BC9. Wind velocities corresponding to each case are shown. Wave period changes little in the southernmost half of the bay.

and H_s (Fig. 5) and also between energy dissipation and mean absolute period (Fig. 6). This is especially notable in the areas where appreciable attenuation occurs. For example, at the bay entrance, where water depth shoals by 6 m, high rates of energy dissipation and high values of H_s are observed. It should also be noted that the bathymetric shoaling here may also contribute to swell attenuation.

Three more cases were run to assess the separate effects of bottom friction, depth-induced breaking and whitecapping on H_s and the wave spectra. The differences between the base case BC1 and the sequential elimination of each dissipation factor were rather small (not shown). Exclusion of depth-induced wave breaking and whitecapping produced essentially the same results as with the inclusion of these two agents. The most important factor of those three was bottom friction, attenuating H_s around the shallow portions of the bay. However, the elimination of these three factors from the simulation did not affect the wave spectra in an appreciable way (Fig. 8). The energy density spectra for these cases were almost identical to the BC1 case for waves with

frequencies < 0.25 Hz. Very small differences in the spectra were apparent for waves with frequencies > 0.25 Hz. The similarity between the two panels in Fig. 8 indicates that attenuation (or energy dissipation) of the waves as they propagated toward the head was only slightly affected by bottom friction, depth-induced breaking or whitecapping. The quantitative contribution of these attenuating factors is determined at the end of this section.

Additional reasons for the low-frequency waves to attenuate can be refraction and shoaling. Because both refraction and shoaling are depth-dependent phenomena, the bathymetry of the bay was changed and four more cases with flat bottom were run. The wind velocity and wave forcing were the same as the base case BC1. The flat bathymetries had depths of 2, 25, 50 and 100 m for each of the 4 additional cases. Depths were chosen to determine the behavior of the bay in shallow, intermediate and deep water conditions (Dean and Dalrymple, 1991). Only the case with a depth of 50 m is shown, all others are consistent. Results over a depth of 2 m represent shallow water waves, those over 25

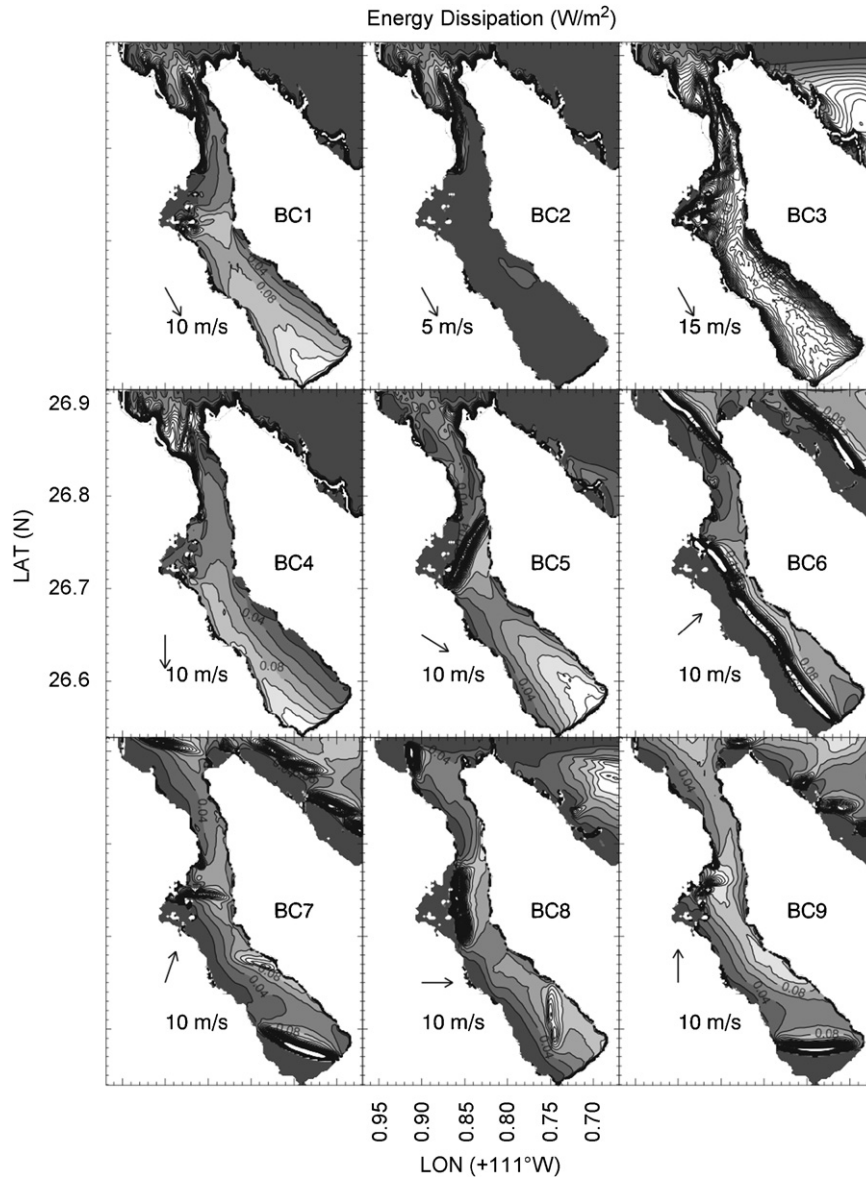


Fig. 7. Energy dissipation (contours at intervals of 0.02 W/m^2) for BC1 to BC9. Wind velocities corresponding to each case are shown. Strongest dissipation occurs in areas with open fetch.

and 50 m indicate intermediate depths and over 100 m represent deep water conditions. These simulations indicate that low-frequency waves can propagate further into the bay as the water depth increases (i.e., as the waves propagate in deeper water) but up to a certain depth, only. For instance, in shallow water (depth of 2 m), 10 s waves were dissipated after 500 m into the bay from the mouth, but for intermediate depths of 25 and 50 m, they intruded up to ~ 20 km. For a depth of 100 m, low-frequency waves disappeared 22 km before reaching the head. Fig. 9 (upper panel) shows the wave spectra for the case with 50 m flat bottom. In this case, low-frequency waves intrude further into the bay than in BC1 (e.g. upper panel of Fig. 8) but attenuate practically halfway. This indicates that refraction plays a role, albeit secondary, in attenuating long-period waves in this bay.

Swell waves did not reach the head of the bay even after eliminating bottom friction and refraction. Concepción Bay has a curved geometry that causes waves to be blocked as they propagate, especially at latitudes $26^\circ 42' 36''$ and $26^\circ 46' 48''$. At locations where the propagation of low-frequency waves was blocked, energy was distributed laterally, perpendicular to the

dominant wave direction and thus waves attenuated. An additional case was then run to assess the effect of bay geometry. In this case, the bay geometry was replaced by a rectangular flat channel with a width of 7 km, a length of 42 km, and a depth of 30 m, dimensions inspired by Concepción Bay. Waves were prescribed to propagate southward (from 0°T) at the northern boundary of the bay with a wave height of 1.5 m, a wave period of 10 s and a wave directional spreading of 5° . This wave direction was prescribed to enable a propagation perpendicular to the axis of the channel. Winds were also southward at 10 m/s. In addition to these settings, bottom friction was reduced by assigning the coefficient of JONSWAP to be $0.0001 \text{ m}^2/\text{s}^3$. The spectral energy density for this case clearly shows the swell waves propagating all the way to the head of the basin (bottom panel of Fig. 9) with little or no attenuation. In fact, waves of all frequencies propagate throughout the basin. This experiment indicates that the geometry of Bahía Concepción blocks the propagation of long waves generated outside the bay.

The wave transformations simulated by different experiments are summarized with the wave spectral energy density from the

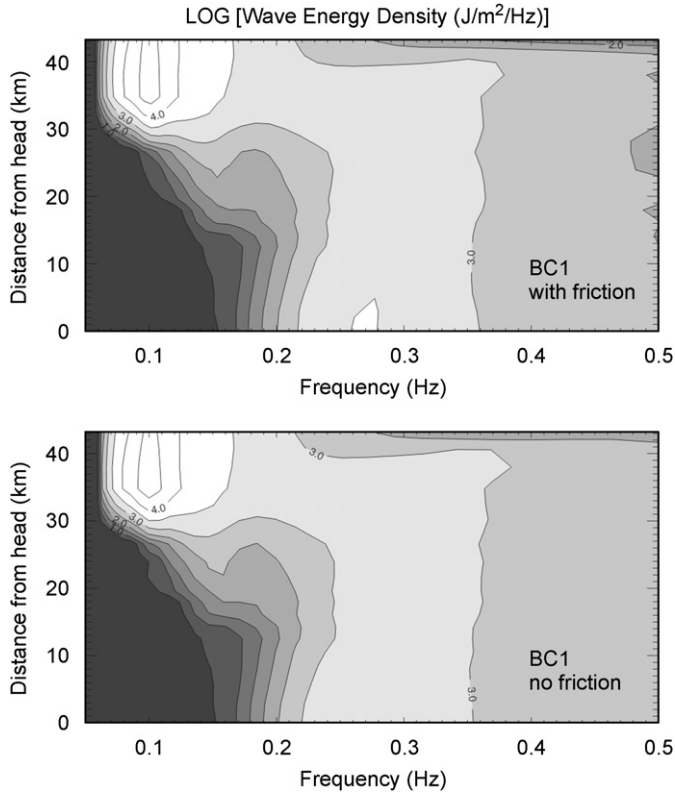


Fig. 8. Logarithm of the wave spectral energy density (contours at intervals of $10^{0.5} \text{ J/m}^2$) throughout the bay (at points shown in Fig. 1) for BC1 (upper panel) and the case without bottom friction, depth-induced breaking or whitecapping (lower panel). Frictional effects from the latter 3 agents cause rather small modifications to the wave field.

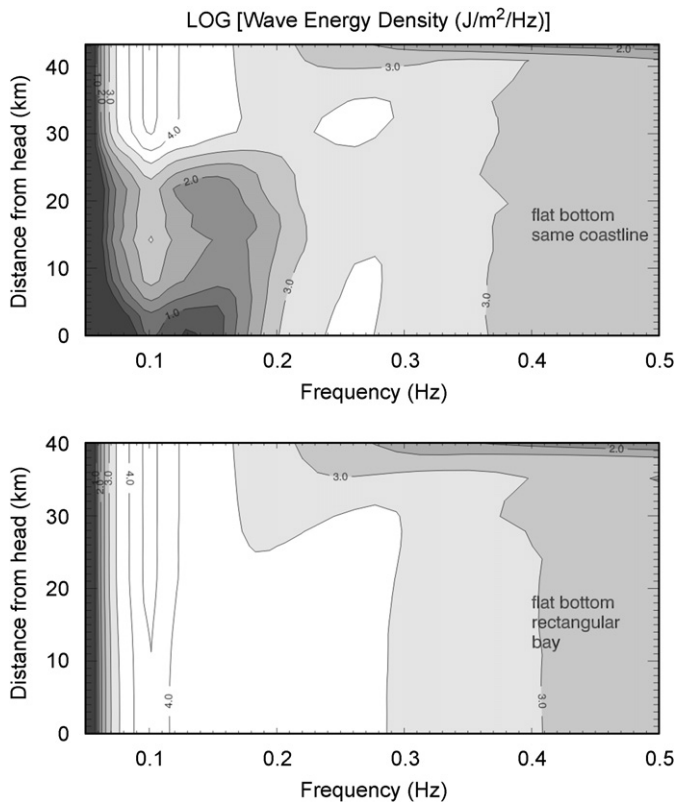


Fig. 9. Same as Fig. 8 but for a flat-bottom Concepción Bay (upper panel) and a rectangular channel (lower panel). Long waves make it all the way to the bay head.

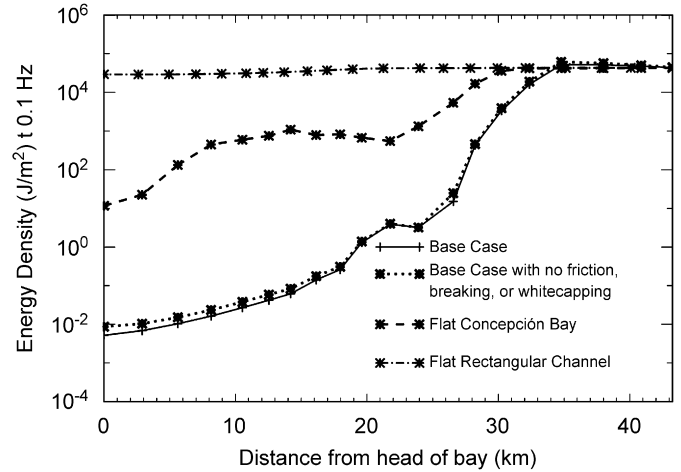


Fig. 10. Wave spectral energy density of the 0.1 Hz (10s) waves as a function of distance from the bay head for various cases. Note the logarithmic scale in the ordinate. All cases, except for the Flat Rectangular Channel, show vanishing of 0.1 Hz waves by a distance of ~ 20 km from the bay mouth. The dotted line represents dissipative effects from friction (6%); the dashed line depicts dissipation from refraction (5%); and the dash-dot line portrays dissipation from blocking (89%).

bay head to the mouth for waves of 0.1 Hz (Fig. 10). The cases illustrated are (a) the base case BC1 (Fig. 8 upper panel); (b) BC1 without bottom friction, depth-induced breaking and whitecapping (Fig. 8 lower panel); (c) flat bottom with a water depth of 50 m (Fig. 9 upper panel); and (d) rectangular bay without bottom friction (Fig. 9 lower panel). With the original bay geometry, even for the most basic case where bottom friction, depth-induced breaking, whitecapping, and refraction were eliminated (flat bottom of 50 m), the spectral energy density curve decreases from the entrance to the head. The distance of 30 km from the head, right in the area where the bay is narrowest and with greatest curvature, seems to be where wave dissipation turns on. Integrating the area under each curve yields an energy density of $5.32 \times 10^8 \text{ J/m}$ for the base case BC1 and $5.90 \times 10^8 \text{ J/m}$ for BC1 without friction, breaking or whitecapping. This represents an attenuation of $0.58 \times 10^8 \text{ J/m}$ caused by friction, breaking and whitecapping. The integrated energy density of 0.1 Hz waves over a flat-bottomed Concepción Bay is $6.37 \times 10^8 \text{ J/m}$, a difference of $0.47 \times 10^8 \text{ J/m}$ with respect to the frictionless case. Such difference may be attributed to losses of wave energy density from refraction. Finally, the dissipation of 0.1 Hz waves in a rectangular basin of roughly the same dimensions as Concepción Bay, is minimal throughout the domain. The wave energy density throughout the basin in this case is $15.09 \times 10^8 \text{ J/m}$, a difference of $8.72 \times 10^8 \text{ J/m}$ with respect to the flat basin with the same coastline as Concepción Bay. This energy loss can be ascribed to the blocking effect of the coastline.

The energy losses credited to frictional effects (plus breaking and whitecapping), refraction and blocking on 0.1 Hz waves amounted then to $9.77 \times 10^8 \text{ J/m}$ ($8.72 \times 10^8 \text{ J/m} + 0.47 \times 10^8 \text{ J/m} + 0.58 \times 10^8 \text{ J/m}$). Out of those energy losses, bottom friction, whitecapping and depth-induced breaking contributed $\sim 6\%$ and refraction contributed $\sim 5\%$ to swell attenuation. The latter two mechanisms acted within the first few kilometers from the bay mouth, where waves were not blocked by land. Most of the contribution to swell attenuation, $\sim 89\%$, was caused by coastline blocking at the region of the bay with greatest coastline curvature, i.e., where it changes orientation.

4. Conclusions

Both *in-situ* data and model results show that ocean swell waves were attenuated as they propagated into an elongated bay, Concepción Bay, and that they vanished before reaching the head. Locally, generated high-frequency wind waves appeared throughout the bay as also indicated by both observational and model results. Eventhough the data were not collected to study surface waves, results obtained from the model experiments verified that the pattern suggested by the observations was reliable. This study in Concepcion Bay should help in the understanding of wave propagation processes in other embayments of the world, where the wave blocking mechanism should be explored further.

The processes that caused attenuation of swell waves in this elongated bay were bottom friction, depth-induced breaking and whitecapping, refraction and wave blocking. Geometric configuration was the main reason for swell waves not reaching the head of the bay. Waves were blocked by the coastline especially beyond 20 km into the bay. According to the energy-based calculations, 89% of the swell waves were blocked by the coastline before reaching the head. The contribution of refraction was ~5%, while the combined role of bottom friction, depth-induced wave breaking and whitecapping was ~6%.

Acknowledgments

This study was funded by NSF project OCE-0551923. The help on the field by G. Gutierrez, H. Torres, M.A. Cosío, C. Winant, K. Winters, A. Ponte and J. Ruettgers was pivotal for the data collection and is gratefully acknowledged. The comments of R. Dean, A. Kennedy and two anonymous reviewers are greatly appreciated. A. Sheremet suggested and helped in the use of SWAN for which we thank him.

References

- Abreu, M., Larraza, A., Thornton, E., 1992. Nonlinear transformation of directional wave spectra in shallow water. *Journal of Geophysical Research* 97, 15,579–15,589.
- Ardhuin, F., O'Reilly, W.C., Herbers, T.H.C., Jessen, P.F., 2003a. Swell transformation across the continental shelf. Part I: attenuation and directional broadening. *Journal of Physical Oceanography* 33, 1921–1939.
- Ardhuin, F., Herbers, T.H.C., Jessen, P.F., O'Reilly, W.C., 2003b. Swell transformation across the continental shelf. Part II: validation of a spectral energy balance equation. *Journal of Physical Oceanography* 33, 1940–1953.
- Badan-Dangon, A., Dorman, C.D., Merrifield, M.A., Winant, C.D., 1991. The lower atmosphere over the Gulf of California. *Journal of Geophysical Research* 96 (C9), 16,877–16,896.
- Booij, N., Ris, R.C., Holthuijsen, L.H., 1999. A third-generation wave model for coastal regions, 1, model description and validation. *Journal of Geophysical Research* 104 (C4), 7649–7666.
- Boon, J.D., Green, M.O., Suh, K.D., 1996. Bimodal wave spectra in lower Chesapeake Bay, sea bed energetics and sediment transport during winter storms. *Continental Shelf Research* 16, 1965–1988.
- Chawla, A., Kirby, J.T., 2002. Monochromatic and random wave breaking at blocking points. *Journal of Geophysical Research* 107 (C7).
- Collins, J.L., 1972. Prediction of shallow water spectra. *Journal of Geophysical Research* 77 (15), 2693–2707.
- Dean, R.G., Dalrymple, R.A., 1991. *Water Wave Mechanics for Engineers and Scientists*, second ed. Prentice-Hall, Englewood Cliffs, NJ.
- Hasselmann, K., Barnett, T.P., Bouws, E., Carlson, H., Cartwright, D.E., Enke, K., Ewing, J.A., Gienapp, H., Hasselmann, D.E., Kruseman, P., Meerburg, A., Müller, P., Olbers, D.J., Richter, K., Sell, W., Walden, H., 1973. Measurements of wind-wave growth and swell decay during the joint north sea wave project (JONSWAP). *Deutschen Hydrographischen Zeitschrift* 12, A8.
- Jeffreys, J., 1924. On the formation of the waves by wind. *Proceedings of the Royal Society London A*, 107–189.
- Long, R.B., 1973. Scattering of surface waves by an irregular bottom. *Journal of Geophysical Research* 78 (33), 7861–7870.
- Long, C.E., Oltman-Shay, J.M., 1991. Directional characteristics of waves in shallow water. Technical Report CERC-91-1, US Army Engineer Waterways Experiment Station.
- Madsen, O.S., Poon, Y.K., Graber, H.C., 1988. Spectral wave attenuation by bottom friction: theory. In: *Proceedings of the 21st International Conference on Coastal Engineering*, ASCE, pp. 492–504.
- Mitsuyasu, H., 1997. On the contribution of swell to sea surface phenomena. *International Journal of Offshore and Polar Engineering* 4 (V7), 241–245.
- Pawka, S.S., Inman, D.L., Guza, R.T., 1984. Island sheltering of surface gravity waves: model and experiment. *Continental Shelf Research* 3 (1), 35–53.
- Ris, R.C., Holthuijsen, L.H., Booij, N., 1999. A third-generation wave model for coastal regions, 2, verification. *Journal of Geophysical Research* 104 (C4), 7667–7682.
- Shyu, J.H., Phillips, O.M., 1990. The blockage of gravity and capillary waves by longer waves and currents. *Journal of Fluid Mechanism* 217, 115–141.
- Smith, M.J., Stevens, C.L., Gorman, R.M., McGregor, J.A., Neilson, C.G., 2001. Wind-wave development across a shallow intertidal estuary: a case study of Manukau Harbour, New Zealand. *New Zealand Journal of Marine and Freshwater Research* 35, 985–1000.
- Soomere, T., 2005. Wind wave statistics in Tallinn Bay. *Boreal Environment Research* 10, 103–118.
- Thornton, E.B., Guza, R.T., 1983. Transformation of wave height distribution. *Journal of Geophysical Research* 88 (C10), 5925–5938.
- Ts'o, P.Y., Barsky, B.A., 1987. Modeling and rendering waves: wave-tracing using beta-splines and reflective and refractive texture mapping. *ACM Transactions on Graphics (TOG) Archive* 6 (3), 191–214.
- Wu, C.S., Thornton, E.B., 1989. Transformation of water waves in Monterey Bay, coastal zone '89. In: *Proceeding of the Sixth Symposium on Coastal and Ocean Management*, vol. 3, pp. 2837–2849.